Journal of Fluorescence, Vol. 4, No. 2, 1994

Distributions of Fluorescence Decay Times for Synthetic Melittin in Water–Methanol Mixtures and Complexed with Calmodulin, Troponin C, and Phospholipids

Joseph R. Lakowicz,[1] Ignacy Gryczynski,[1] Wieslaw Wiczk,[1,3] and Michael L. Johnson[2]

Received July 26, 1993; revised February 1, 1994; accepted April 6, 1994

Frequency-domain measurements of the intensity decays of melittin were used to recover the distribution of decay times displayed by its single tryptophan residue. Melittin was examined in the monomeric random coil state (water), in the monomeric α-helical state (water–methanol), in the tetrameric state, and with 6 *M* guanidine hydrochloride. In the presence of denaturant, where melittin is expected to be devoid of secondary structure, we observed a narrow distribution of lifetimes, similar to a double-exponential decay. In water the intensity decay of melittin was found to be described better by the distribution of decay times, which became progressively wider as the amount of α-helix was increased by the methanol cosolvent or upon formation of the α-helical tetrameric state. We also examined the intensity decays of melittin when complexed with calmodulin, troponin C, or lipid vesicles of 1-palmitoyl-2-oleyl-L-α-phosphatidylcholine (POPC). The lifetime distributions of the complexes with lipid were comparable to those observed in methanol–water, suggesting a similarity of the structure and/or dynamics of the environment surrounding the tryptophan residue. A broad lifetime distribution was observed for the melittin–calmodulin complex, suggesting a rigid structure and/or heterogeneity in the form of the complex. The lifetime distribution of the melittin–troponin C complex was more narrow, suggesting a more uniform structure, at least in the region surrounding the tryptophan residue. These results demonstrate that the lifetime distributions of a single tryptophan protein can be a sensitive indicator of the conformational heterogeneity and dynamics of proteins.

KEY WORDS: Melittin; water–methanol; calmodulin; troponin C; phospholipids; fluorescence decay times.

INTRODUCTION

The tryptophan emission decay kinetics of proteins are of interest because of their sensitivity to the structural and dynamic features of proteins. However, it is difficult to correlate the decay kinetics with known features of protein structure and dynamics. In an effort to elucidate this linkage we examined the decay kinetics of the single tryptophan residue of melittin. This amphipathic peptide from bee venom was chosen because it exists in a variety of conformational states, depending upon ionic strength and solvent polarity [1–5]. Additionally, melittin forms complexes with calmodulin (CaM)[4] [6–8], troponin C (TnC) [9,10], and lipids [11–13], apparently due to hydrophobic interactions between the nonpolar patches of

[1] Department of Biological Chemistry, University of Maryland, School of Medicine, 108 North Greene Street, Baltimore, Maryland 21201.
[2] Department of Pharmacology, University of Virginia, Charlottesville, Virginia 22908.
[3] Present address: Institute of Chemistry, University of Gdansk, Gdansk 6, Sobieskiego 18, Poland.

[4] Abbreviations used: CaM, calmodulin; GuHCl, guanidine hydrochloride; NATA, *N*-acetyl-L-tryptophanamide; mel, melittin; POPC, 1-palmitoyl-2-oleyl-L-α-phosphatidylcholine; TnC, troponin C.

1053-0509/94/0600-0169$07.00/0

these macromolecules and that of melittin in the α-helical state. The conformational variability displayed by melittin thus provides an opportunity to compare the tryptophan emission decay kinetics in a variety of conformations.

The fluorescence intensity decay of proteins, even those containing a single tryptophan residue, are generally more complex than a single exponential [14,15]. The intensity decays are most frequently analyzed in terms of discrete exponentials [15,16] i.e., the multiexponential model. Although rarely stated explicitly, one reason for the extensive use of the multiexponential model is that it is versatile enough to fit the most complex intensity decays. Additionally, it is intuitively straightforward and computationally simple. Recently, the use of continuous distributions of decay time has been proposed as an alternative to the multiexponential model [17–30]. Lifetime distributions have been used to investigate the photophysics of molecules adsorbed on surfaces [19] and molecules dissolved in mixtures of polar and nonpolar solvents [23,26] and of the tryptophan decay kinetics of proteins [22,28–30]. In the case of ribonuclease T_1 [29], the intensity decay was found to be a single exponential in the native solution state and to become increasingly heterogeneous (i.e., broader distribution) as unfolding and/or conformational heterogeneity was induced by heating or denaturants. The present investigation is intended to extend these studies by determining the effects of different environments on the lifetime distributions of the single tryptophan residue in melittin.

THEORY

For a multiexponential decay the impulse response $[I(t)]$ is given by

$$I(t) = \sum_i \alpha_i e^{-t/\tau_i} \tag{1}$$

where α_i are the preexponential factors and τ_i the decay times, $\sum_i \alpha_i = 1.0$. Alternatively, the intensity decays can be modeled using a distribution of decay times. We assumed that the individual components were distributed as a Lorentzian,

$$\alpha_i^0(\tau) = \frac{1}{\pi} \frac{\Gamma_i/2}{(\tau - \bar{\tau}_i)^2 + (\Gamma_i/2)^2} \tag{2}$$

where Γ_i is the full-width at half-maximum, $\bar{\tau}_i$ is the central value of the ith distribution, and $\int \alpha_i^0(\tau) d\tau = 1$. According to this definition, $\alpha_i^0(\tau)$ is a shape-factor for the ith component in the distribution. A distribution with a single component is referred to as a unimodal distribution, two components as a bimodal distribution, etc. In the case of two or more components, the distribution is given by

$$\alpha(\tau) = \sum_i g_i \alpha_i^0(\tau) = \sum_i \alpha_i(\tau) \tag{3}$$

where g_i represents the τ-integrated amplitude of the ith component $\sum_i g_i = 1.0$. The intensity decay is then given by the integral equation

$$I(t) = \int_{\tau=0}^{\infty} \alpha(\tau)\, e^{-t/\tau}\, d\tau \tag{4}$$

We measured the intensity decays using the frequency-domain method [31,32]. The measured quantities are the phase angle (ϕ_ω) and modulation (m_ω) of the emission, relative to the intensity-modulated excitation, measured over a range of circular modulation frequencies (ω). Irrespective of the model assumed for the intensity decay, the frequency-domain data can be calculated from the sine and cosine transforms of the intensity decay,

$$N_\omega = \frac{\int_0^\infty I(t) \sin \omega t dt}{\int_0^\infty I(t)\, dt} \tag{5}$$

$$D_\omega = \frac{\int_0^\infty I(t) \cos \omega t dt}{\int_0^\infty I(t)\, dt} \tag{6}$$

The calculated (c) values of the phase angle ($\phi_{c\omega}$) and the demodulation ($m_{c\omega}$) are given by

$$\tan\phi_{c\omega} = \frac{N_\omega}{D_\omega} \tag{7}$$

$$m_{c\omega} = [N_\omega^2 + D_\omega^2]^{1/2} \tag{8}$$

The parameters (α_i and τ_i, g_i, $\bar{\tau}_i$, and Γ_i) are varied to yield the best fit between the data and the calculated values, as indicated by a minimum value for the goodness-of-fit parameter χ_R^2 [35,36],

$$\chi_R^2 = \frac{1}{\nu}\sum_\omega \left[\frac{\phi_\omega - \phi_{\omega c}}{\delta\phi}\right]^2 + \frac{1}{\nu}\sum_\omega \left[\frac{m_\omega - m_{\omega c}}{\delta m}\right]^2 \tag{9}$$

where ν is the number of degrees of freedom and $\delta\phi$ and δm are the uncertainties in the phase and modulation values, respectively. The number of degrees of freedom is given by $\nu = N - n - 1$, where N is the number of data points and n is the number of fitted parameters. In our analyses we used the values $\delta\phi = 0.2°$ for phase and $\delta m = 0.005$ for modulation.

MATERIALS AND METHODS

Frequency-domain measurements were performed using a gigahertz fluorometer described previously [33,34]. The laser beam was expanded to about 5 mm in diameter to decrease its local intensity. Melittin was excited at 298 nm and the emission was observed through a 360-nm interference filter. Intensity decays were measured using magic-angle polarization conditions.

Synthetic melittin was prepared using standard procedures for solid-phase peptide synthesis, as described previously [37], followed by purification by reverse-phase HPLC on a C_8 column. CaM was from bovine testes and was a gift from Professor Robert Steiner, University of Maryland, Baltimore County. TnC was from rabbit skeletal muscle and was a gift from Professor Herbert Cheung, University of Alabama.

All solutions (without lipid) were in 5 m*M* MOPS, pH 7, containing 1 m*M* Ca^{2+}. Melittin tetramers were obtained using the same buffer with the addition of 2 *M* NaCl. The concentration of melittin was 2×10^{-5} *M* (obtained from the absorbance at 280 nm, $\epsilon = 5500$ M^{-1} cm^{-1}). The concentration of TnC was 2.4×10^{-5} *M* [ϵ(278 nm) = 4140 M^{-1} cm^{-1}] and that of CaM was 2.4×10^{-5} [ϵ(278 nm) = 3340 M^{-1} cm^{-1}]. For solutions containing lipid (1 m*M* POPC) the melittin concentration was 1×10^{-5} *M*, in 10 m*M* MOPS, pH 7, containing 10 m*M* KCl. Under these conditions the membrane-bound form of melittin is expected to be monomeric [4]. The CD spectra were obtained using an Aviv 60 SD spectrophotometer. The percentage α-helix was calculated using least-squares, using the basis spectra described previously [38]. All measurements were performed at 20°C.

RESULTS AND DISCUSSION

Fluorescence spectra of synthetic melittin in water–methanol mixtures are shown in Fig. 1. We observed an increase in fluorescence intensity and a small blue shift as the percentage of methanol was increased. NMR, as well as CD, data for melittin [5] indicate a nearly complete α-helical structure in 80% methanol. We suspect that the increased intensity in methanol is due to the inhibition of quenching by adjacent amino acids, as the protein adopts an elongated shape and the polar residues are clustered on the side of the α-helix opposite from the tryptophan residue [39]. Melittin contains a high percentage of lysine residues, and protonated amines are typically quenchers of tryptophan fluorescence. The blue shift is probably due to the decreased polarity of the solvent as methanol is added. In GuHCl the intensity is decreased about 12% and the emission shifted slightly to longer wavelengths, relative to the emission in water. This result is consistent with the presence of some residual structure in water and disruption of this structure by 6 *M* GuHCl.

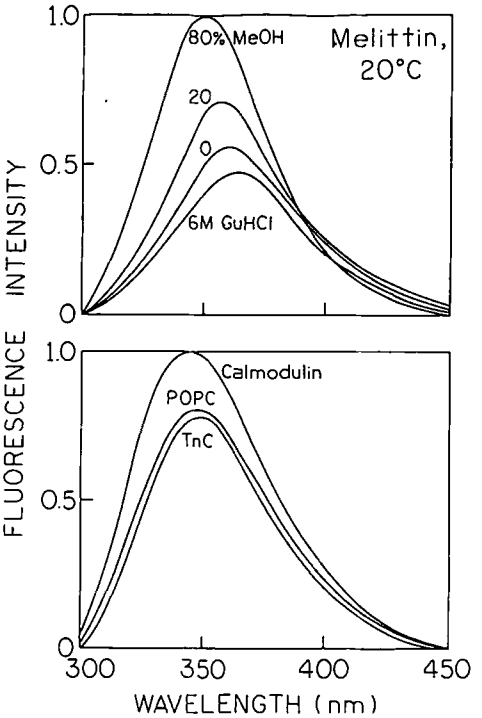

Fig. 1. Fluorescence spectra of synthetic melittin in water–methanol mixtures (top) and melittin bound to CaM, TnC, or POPC (bottom).

The fluorescence decay of melittin is strongly heterogeneous and generally requires a triple-exponential model (which contains five variable parameters, α_1, α_2, τ_1, τ_2, and τ_3) to obtain an adequate fit [40–43]. Complex and/or multiexponential intensity decays for melittin have been observed previously using frequency-domain [40,41] or time-domain [42,43] measurement. While the exact values of α_i and τ_i differ slightly among these reports, there is general agreement on the intensity decay of melittin.

We analyzed our frequency-domain data for melittin using the bimodal Lorentzian model, which also contains five variable parameters (g_1, Γ_1, Γ_2, $\bar{\tau}_1$, and $\bar{\tau}_2$). In general, the quality of the fits, as judged from the values of χ^2_R, was similar for these models. Hence, the selection of the bimodal Lorentzian, instead of the triple-exponential model, must be regarded as arbitrary until additional data allow one to distinguish between the two models with five parameters. One reason for selecting the lifetime distribution model is to avoid the inference that these exist only as a discrete number of conformations, which seems unlikely for the progressively folded state of melittin.

Phase and modulation data for melittin in the mixture containing 80% methanol are presented in Fig. 2. The solid line indicates the best fit for the bimodal Lorentzian, resulting in half-widths of 0.26 and 2.34 ns. To determine whether such widths were in fact determined by the data, we fit the data using fixed and narrow half-widths. The dashed line shows the best fit when the Γ_i's were held fixed at the narrow value of 0.01 ns. The latter fit, which is essentially equivalent to the double-exponential model, is less satisfactory. The value of χ^2_R is elevated threefold. The deviations (lower panels; o) show some increase and are moderated systematically with frequency. Hence, the intensity decay data for melittin in 80% methanol cannot be explained by the double-exponential model, but a bimodal Lorentzian with nonzero half-widths is adequate to account for the data.

The bimodal Lorentzian distributions resulting from the best fit to the frequency-domain data for melittin in 80% methanol are shown graphically in Fig. 3 (bottom panel), and the recovered parameters for all the methanol–water mixtures are summarized in Table I. It appears that the lifetime distribution becomes progressively broader as an α-helical structure is induced by methanol. The lifetime distribution in water (middle panel) is considerably more narrow than that in 80% methanol. The effect of GuHCl is consistent with this observation in that disruption of residual structure by 6 *M* GuHCl resulted in the narrowest lifetime distribution (top panel). Hence, it appears that the occurrence of secondary structure in melittin results in a distribution of lifetimes. Methanol was chosen to induce helix formation because, as opposed to high ionic strength, the melittin remains in the monomeric state. It should be noted that similarly

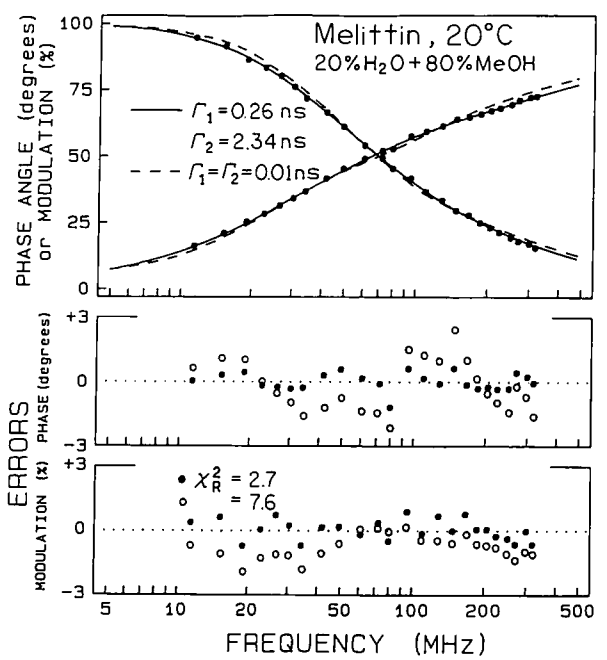

Fig. 2. Phase and modulation data for synthetic melittin in 20% H_2O + 80% MeOH. The solid line and filled circles show the best fit to a bimodal Lorentzian; and dashed line and circles show the fit when Γ_1 and Γ_2 were held constant at the narrow value of 0.01 ns.

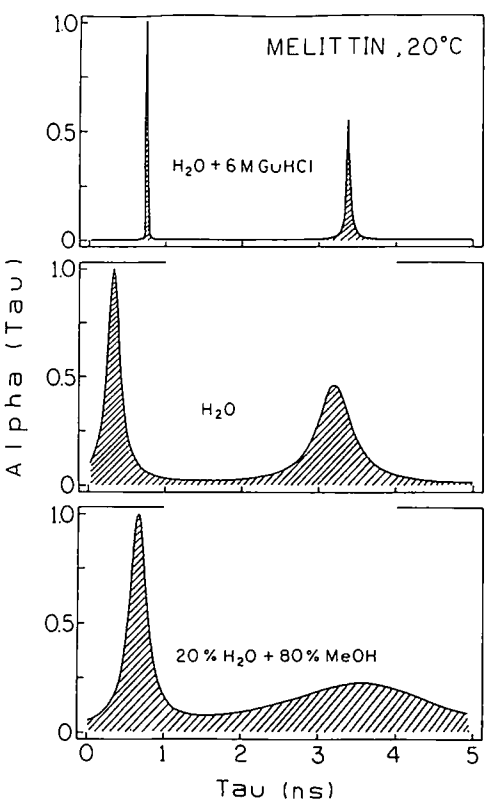

Fig. 3. Lifetime distributions for synthetic melittin in H_2O + 6 *M* GuHCl (top), H_2O (middle), and a mixture of 20% H_2O + 80% MeOH (bottom).

Table I. Lifetime Distribution Parameters for Synthetic Melittin in Water–Methanol Mixtures

% MeOH	$\bar{\tau}_i$ (ns)		Γ_i (ns)		g_i	χ_R^{2a} 1 (uni)	2 (bi)	3 (exp)
0	0.23	(0.15)[b]	0.21	(0.08)	0.49			
	3.07	(0.07)	0.53	(0.18)	0.51	67.6	1.4	1.4
—[c]	0.10	—	⟨0.20⟩	—	0.48			
	2.61	—	⟨2.20⟩	—	0.52		6.6	
20	0.39	(0.05)	0.09	(0.26)	0.36			
	3.37	(0.08)	0.84	(0.35)	0.64	69.7	1.3	1.3
40	0.51	(0.02)	0.01	(0.66)	0.28			
	3.41	(0.07)	1.64	(0.12)	0.72	34.8	2.4	2.2
60	0.65	(0.04)	0.01	(0.29)	0.27			
	3.38	(0.22)	2.26	(0.24)	0.73	12.9	2.3	2.2
80	0.67	(0.04)	0.26	(0.39)	0.34			
	3.56	(0.28)	2.34	(0.33)	0.66	12.2	2.9	2.8
100	0.50	(1.6)	0.20	(0.42)	0.10			
	3.40	(0.14)	2.28	(0.14)	0.90	1.0	0.9	0.9
—[c]	1.09	—	⟨0.21⟩	—	0.25			
	4.12	—	⟨0.53⟩	—	0.71			
0 + 6 *M* GuHCl	0.76	(0.07)	0.01	(0.41)	0.28		2.8	
	3.38	(0.09)	0.08	(0.11)	0.72	14.7	1.6	1.4

[a] The values of χ_R^2 are for the uni- and bimodal Lorentzian distributions, and for the triple exponential (exp) model.
[b] The values in parentheses are the uncertainties estimated from the least-squares analysis [49].
[c] These are the cross-fits with the half-widths held constant (angle braces) at the indicated values.

narrow lifetime distributions were observed for NATA in water [44], where the tryptophan residue is obviously not in a region of secondary structure.

The correlation between the width of the lifetime distributions and the extent of helical structures is shown in Fig. 4, where we plotted the width of the second component (Γ_2) versus the percentage of methanol. Also shown are the percentages of α-helical structure (---), as estimated from the CD spectra [38]. It is apparent that the width increases in a manner similar to the percentage of the α-helix.

Similar results were observed when the α-helical state was induced by self-association of melittin into tetramers. Once again, the width of the widths of the lifetime distribution increased upon formation of the α-helical structure. This distribution is probably not the result of the close proximity of tryptophan residue in the tetramer, as earlier studies provided strong evidence against energy transfer in the tetrameric state [40].

Melittin (MW 2840) is known to form complexes and adopt an α-helical structure upon complexation with proteins and/or hydrophobic surfaces. We note that these complexes provide a unique opportunity to study a single tryptophan protein in the presence of other proteins and the effects of the structure and/or strain induced in the melittin structure due to binding with these larger proteins (MW near 16,800). Additionally, the single tryptophan of melittin can be observed without interference from these proteins because CaM and TnC (and of course POPC) lack tryptophan residues. Hence, we examined the lifetime distribution of melittin when complexed with CaM [6–8], TnC [9,10], and lipid vesicles of POPC [11–13]. Complex formation of melittin with these proteins was demonstrated from the anisotropy decays (Table II). In the monomeric and tetrameric states melittin displays overall correlation times near 1.7 and 3.6 ns, respectively, with a substantial fraction of the anisotropy decay being lost through subnanosecond motions. Upon the addition of CaM (MW 16,800) or TnC the subnanosecond motions are mostly damped, and the overall correlation time increases to about 6 ns. A correlation time of 7 ns is expected for such a complex with a molecular weight near 19,640 with 10–20% hydration [7]. The presence of the global motion is easily seen in the frequency-domain anisotropy data (Fig. 5). The anisotropy decay for melittin with POPC is characteristic of that found previously for membrane-bound melittin [45].

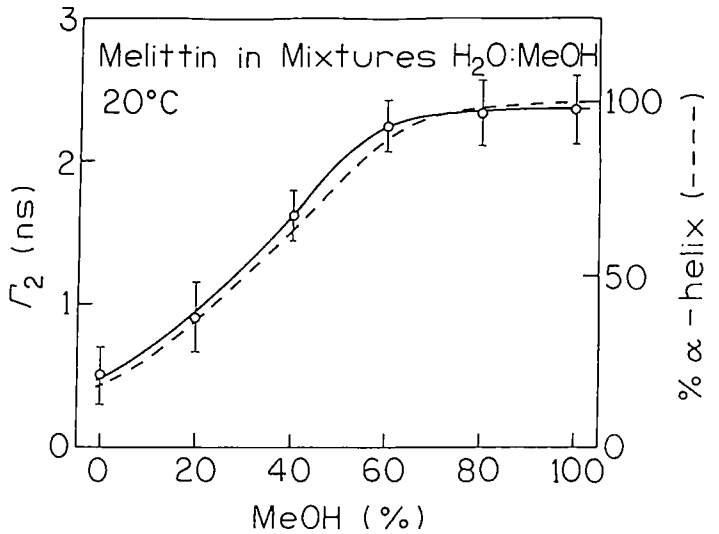

Fig. 4. Dependence of the width of the longer decay time mode (Γ_2) for synthetic melittin upon the volume percentage of methanol in water. The dashed line shows the percentage of α-helix as obtained from the CD spectra [38].

Table II. Anisotropy Decays of Melittin

Solution/complex	θ_i (ns)	$r_0 g_i$	χ^2_R 1[a]	2	3
H_2O/monomer	0.17	0.193			
	1.73	0.126	14.1	0.9	1.0
6 *M* GuHCl	0.18	0.228			
	1.66	0.093	20.6	1.2	1.2
Tetramer/2 M NaCl	0.08	0.072	5.3	1.3	1.3
	3.62	0.210			
α-Helical/80% methanol	0.23	0.120	25.0	1.3	1.2
	1.77	0.174			
+ CaM	0.26	0.084			
	5.95	0.224	26.1	0.9	0.8
TnC	0.37	0.107	54.8	1.0	1.0
	6.10	0.205			
+ POPC	0.16	0.173			
	1.64	0.058			
	41.04	0.101	88.6	1.6	1.0

[a] Number of correlation times in the anisotropy decay analysis.

We also examined the intensity decays of melittin when bound to CaM, TnC, and POPC vesicles. These emission spectra are shown in Fig. 1 (lower panel). The spectra of melittin bound to calmodulin are similar to those reported for binding of dynorphin (1–17) to calmodulin [46]. The lifetime distributions observed for these melittin–protein and melittin-lipid complexes are shown in Fig. 6. Remarkably different lifetime distributions were observed for these three environments (Table III). When bound to POPC vesicles (Fig. 6, bottom) the width of the second mode is comparable to that found for α-helical melittin (Fig. 3, bottom), and melittin is known to be mostly α-helical when bound to lipids [13]. However, when bound to lipid, melittin displays more of its intensity decay in the short-lifetime region of the distribution. This could be the result of collisional quenching interactions with the lipid head groups. We know from previous studies of collisionally quenched samples that transient effects result in short-lived components when analyzed in terms of lifetime distributions [25].

A remarkably wide and distinct lifetime distribution was observed for melittin complexed to calmodulin (Fig. 6, top). Given the narrow lifetime distribution observed in uniform or dynamically uniform environments (Fig. 3), the wide distribution when complexed with CaM seems to imply a heterogeneous environment for the tryptophan residue. While structural heterogeneity of the melittin–CaM complex has not been reported directly, computer modeling studies of this complex have revealed an imperfect fit between these proteins and that folding of the calmodulin and contraction of the complex occurs upon binding [10]. These strained and/or structurally heterogeneous interactions may be the origin of the wide lifetime distribution seen for this complex. In contrast to the complex with CaM, the lifetime distribution of the melittin–TnC complex is narrower (Fig. 6, middle). This seems surprising given the structural similarity of CaM

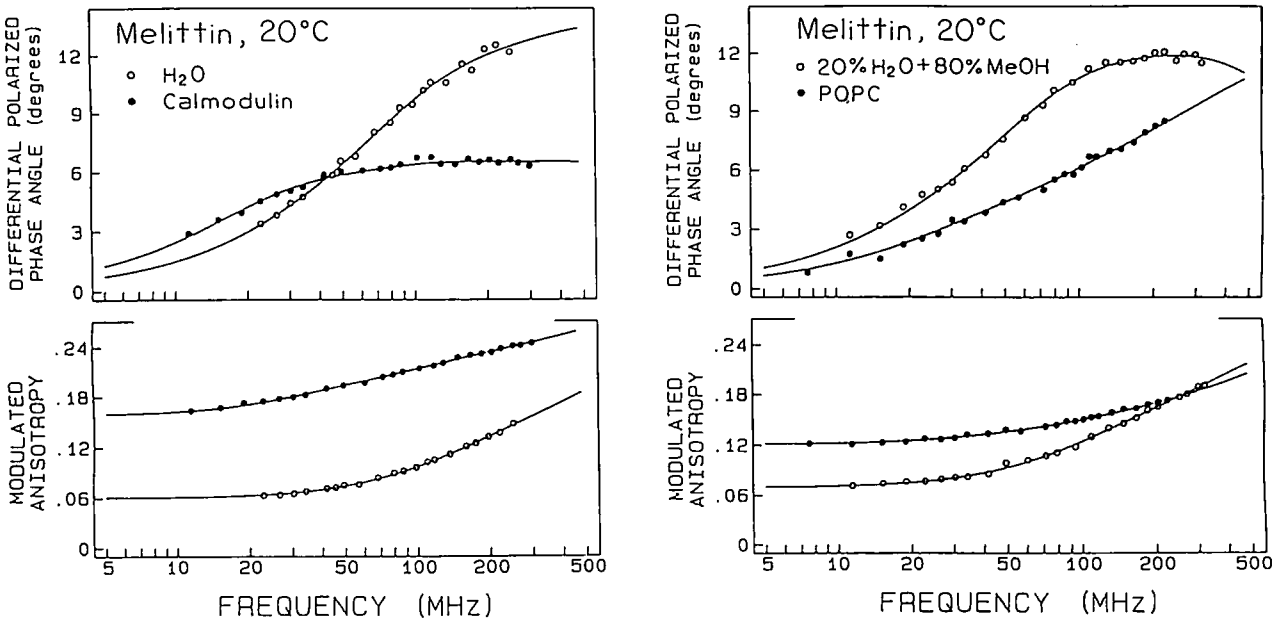

Fig. 5. Frequency-domain anisotropy data for melittin and its complexes.

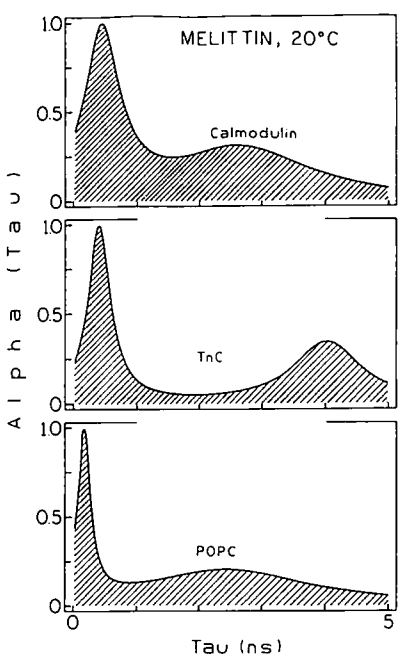

Fig. 6. Lifetime distributions for complexes of melittin with CaM (top), TnC (middle), and POPC (bottom).

and TnC. In fact, the structures of both CaM [47] and TnC [48] appear to contract upon the binding of peptides, which suggests a similar environment for melittin when bound to either protein. An explanation of this difference in the intensity decays of bound melittin must await more detailed spectroscopic and structural information.

We questioned whether the remarkably different lifetime distributions observed for the melittin complexes could be a result of uncertainties and/or instabilities in the fits. Hence, we attempted to see whether the distribution half-width from one complex could be consistent with the data from another complex. To accomplish this test we forced-fit the data from one of the complexes using the half-widths from another complex. The lifetimes and amplitudes were allowed to vary because these differ among the complexes. One example is shown in Fig. 7, where we attempted to fit the melittin–TnC data using the half-widths observed for the melittin–POPC complex (Fig. 7). In this case, the value of χ^2_R is elevated 1.7-fold. There is a significant amount of freedom in these fits, with three variable parameters (τ_1, τ_2, and g_1), as well as the fixed but nonzero widths which result in a range of decay times. These cross fits demonstrate that the widths from one complex are distinct from the others. This is seen by the elevation in χ^2_R which results from the force fits. For instance, the χ^2_R of the melittin–CaM complex is elevated twofold when using the half-width from the similar melittin–TnC complex (Table III). The χ^2_R values are elevated three- to sixfold when the melittin random coil (0% methanol)

Table III. Lifetime Distribution Parameters for Complexes of Melittin

Conditions	$\bar{\tau}_i$ (ns)		Γ_i (ns)		g_i	χ_R^{2a} 1 (uni)	2 (bi)	3 (exp)
Melittin + CaM	0.45	(0.17)	0.66	(0.86)	0.44			
	2.67	(0.59)	2.64	(0.46)	0.56	5.4	1.1	1.1
—[b]	0.70	—	⟨0.44⟩	—	0.53			
	3.47	—	⟨1.32⟩	—	0.47	—	2.0	—
Melittin + TnC	0.41	(0.13)	0.44	(0.38)	0.48			
	4.03	(0.17)	1.32	(0.41)	0.52	25.2	1.6	1.6
—[b]	0.24		⟨0.24⟩		0.38			
	3.44		⟨3.18⟩		0.62	—	2.8	—
Melittin + POPC	0.17	(0.42)	0.24	(0.25)	0.26			
	2.46	(0.27)	3.18	(0.22)	0.74	5.9	1.0	1.0
—[b]	−1.12	—	⟨0.11⟩	—	0.99			
	3.25	—	⟨1.80⟩	—	0.01	—	1.4	—
Melittin tetramer	0.05	(0.06)	0.11	(0.86)	0.11			
	1.93	(0.08)	1.80	(0.07)	0.89	1.9	1.8	1.6
—[b]	1.32	—	⟨0.66⟩	—	0.79	—	1.4	—
	2.36	—	⟨2.64⟩	—	0.26	—	2.2	—

[a] The values of χ_R^2 are for the uni- and bimodal Lorentzian fits and for the triple-exponential (exp) model.
[b] These are cross-fits with the half-widths held constant (angle braces) at the indicated values.

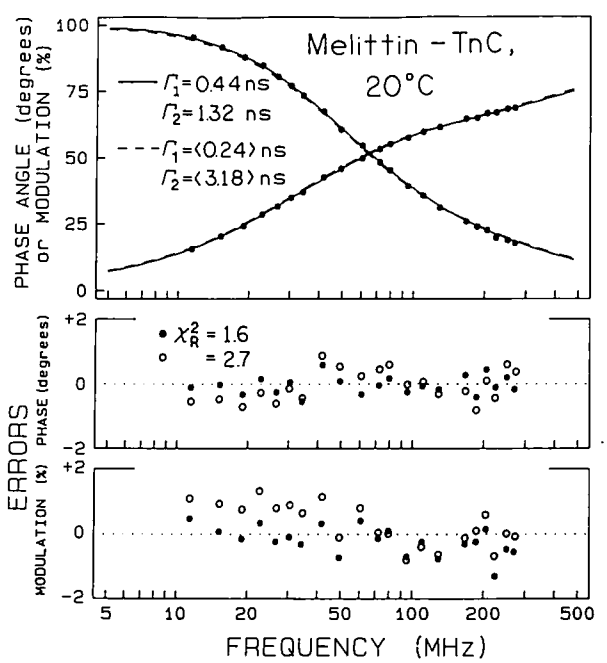

Fig. 7. Frequency-domain data for the melittin–TnC complex. The solid line shows the best fit to the data, and the dashed line the best fit using the widths from the melittin–POPC complex (Table III).

data are cross fit with the α-helix half-width (Table I), and vice versa.

In summary, we found that the lifetime distribution of the intrinsic tryptophan emission of melittin depends upon its conformational state. In general, narrow lifetime distributions were observed in dynamically homogeneous environments, and wider distributions were found in the presence of secondary structure induced by methanol and/or complexation with proteins or lipids.

ACKNOWLEDGMENTS

The authors acknowledge support from the National Science Foundation (DMB-8804931), and the National Institutes of Health (GM-35154). J.R.L. and W.W. also express appreciation for support from the Medical Biotechnology Center at the University of Maryland. The authors give their special thanks to Drs. F. G. Prendergast, A. J. Weaver, and M. D. Kemple (Mayo Foundation, Rochester, Minnesota) for their gift of the melittin.

REFERENCES

1. J. C. Talbot, J. Dufourcq, J. Debong, J. R. Faucon, and C. Lurson (1979) *FEBS Lett.* **102,** 191–193.
2. J. F. Faucon, J. Dufourcq, and C. Lurson (1979) *FEBS Lett.* **102,** 187–190.
3. J. R. Lakowicz, I. Gryczynski, W. Wiczk, F. G. Prendergast, and M. L. Johnson (1990) *Biophys. Chem.* **36,** 99–115.

4. J. C. Talbot, J. F. Faucon, and J. Dufourcq (1987) *Eur. Biophys. J.* **15,** 147–157.
5. R. Bazzo, M. J. Tappin, A. Pastore, T. S. Harvey, J. A. Carver, and I. D. Campbell (1988) *Eur. J. Biochem.* **173,** 139–146.
6. Y. Maulet and J. A. Cox (1983) *Biochemistry* **22,** 5680–5686.
7. R. F. Steiner, L. Marshall, and D. Needleman (1986) *Arch. Biochem. Biophys.* **246,** 286–300.
8. M. Kataoka, J. F. Head, B. A. Seaton, and D. M. Engelman (1989) *Proc. Natl. Acad. Sci.* **86,** 6944–6948.
9. R. F. Steiner and L. Norris (1987) *Arch. Biochem. Biophys.* **254,** 342–352.
10. N. C. J. Strynadka and M. N. G. James (1990) *Proteins Struct. Funct. Genet.* **7,** 234–248.
11. E. Kuchinka and J. Seelig (1989) *Biochemistry* **28,** 4216–4221.
12. C. Dempsey, M. Bitbal, and A. Walts (1989) *Biochemistry* **28,** 6590–6596.
13. G. Beschiaschvili and J. Seelig (1990) *Biochemistry* **29,** 52–58.
14. A. Grinvald and I. Z. Steinberg (1974) *Anal. Biochem.* **59,** 583–598.
15. J. M. Beechem and L. Brand (1985) *Annu. Rev. Biochem.* **54,** 53–71.
16. D. V. O'Connor and D. Phillips (1984) *Time-Correlated Single Photon Counting,* Academic Press, New York.
17. D. R. James and W. R. Ware (1985) *Chem. Phys. Lett.* **120,** 455–459.
18. D. R. James and W. R. Ware (1985) *J. Phys. Chem.* **89,** 5450–5458.
19. D. R. James and W. R. Ware (1985) *Chem. Phys. Lett.* **120,** 460–465.
20. J. R. Alcala, E. Gratton, and F. G. Prendergast (1987) *Biophys. J.* **51,** 587–596.
21. J. R. Alcala, E. Gratton, and F. G. Prendergast (1987) *Biophys. J.* **51,** 597–604.
22. J. R. Alcala, E. Gratton, and F. G. Prendergast (1987) *Biophys. J.* **51,** 925–936.
23. J. R. Lakowicz, H. Cherek, I. Gryczynski, N. Joshi, and M. L. Johnson (1987) *Biophys. Chem.* **28,** 35–50.
24. D. R. James, Y. S. Liu, N. O. Petersen, A. Siemiarczuk, B. D. Wagner, and W. R. Ware (1987) *Proc. SPIE* **743,** 117–122.
25. I. Gryczynski, W. Wiczk, M. L. Johnson, and J. R. Lakowicz (1988) *Biophys. Chem.* **32,** 173–185.
26. I. Gryczynski, W. Wiczk, J. R. Lakowicz, and M. L. Johnson (1989) *J. Photochem. Photobiol. B Biol.* **4,** 159–170.
27. D. R. James, J. R. Turnbull, B. D. Wagner, W. R. Ware, and N. O. Petersen (1987) *Biochemistry* **26,** 6272–6277.
28. E. Bismuto, E. Gratton, and G. Iruce (1988) *Biochemistry* **27,** 2132–2138.
29. I. Gryczynski, M. Eftink, and J. R. Lakowicz (1988) *Biochim. Biophys. Acta* **954,** 244–252.
30. I. Gryczynski, W. Wiczk, G. Inesi, T. Squier, and J. R. Lakowicz (1989) *Biochemistry* **28,** 3490–3498.
31. E. Gratton and M. Limkeman (1983) *Biophys. J.* **44,** 315–324.
32. J. R. Lakowicz and B. P. Maliwal (1985) *Biophys. Chem.* **21,** 61–78.
33. J. R. Lakowicz, G. Laczko, and I. Gryczynski (1986) *Rev. Sci. Instrum.* **57,** 2499–2506.
34. G. Laczko, I. Gryczynski, Z. Gryczynski, W. Wiczk, H. Malak, and J. R. Lakowicz (1990) *Rev. Sci. Instrum.* **61,** 2331–2337.
35. E. Gratton, J. R. Lakowicz, B. Maliwal, H. Cherek, G. Laczko, and M. Limkeman (1984) *Biophys. J.* **46,** 479–486.
36. J. R. Lakowicz, E. Gratton, G. Laczko, H. Cherek, and M. Limkeman (1984) *Biophys. J.* **46,** 463–477.
37. A. J. Weaver, M. D. Kemple, and F. G. Prendergast (1989) *Biochemistry* **28,** 8614–8623.
38. N. Greenfield and G. D. Fasman (1969) *Biochemistry* **8,** 4108.
39. K. T. O'Neil, H. R. Wolfe, Jr., S. Erickson-Viitanen, and W. F. DeGrado (1987) *Science* **236,** 1454–1456.
40. J. R. Lakowicz, H. Cherek, I. Gryczynski, N. Joshi, and M. L. Johnson (1987) *Biophys. J.* **51,** 755–768.
41. J. R. Lakowicz, G. Laczko, I. Gryczynski, and H. Cherek (1986) *J. Biol. Chem.* **261,** 2240–2245.
42. E. John and F. Jahnig (1988) *Biophys. J.* **54,** 817–827.
43. C. D. Tran and G. S. Beddard (1985) *Eur. Biophys. J.* **13,** 59–64.
44. H. Cherek, I. Gryczynski, G. Laczko, M. L. Johnson, and J. R. Lakowicz (1986) *Proceedings of International Symposium on Molecular Luminescence and Photophysics,* Torun, Poland, Sept. 2–5, pp. 124–128.
45. B. P. Maliwal, A. Hermetter, and J. R. Lakowicz (1986) *Biochim. Biophys. Acta* **873,** 173–181.
46. D. A. Malencik and S. R. Anderson (1984) *Biochemistry* **23,** 2420–2428.
47. M. Ikura, G. M. Glore, A. M. Gronenborn, G. Zhu, C. B. Klee, and A. Bax (1992) *Science* **256,** 632–638.
48. S. L. Blechner, G. A. Olah, N. C. J. Strynadka, R. S. Hodges, and J. Trewhella (1992) *Biochemistry* **31,** 11326–11334.
49. M. Straume, S. G. Frasier-Cadoret, and M. L. Johnson (1991) in J. R. Lakowicz (Ed.), *Topics in Fluorescence Spectroscopy, Vol. 2. Principles,* Plenum Press, New York, pp. 177–240.